Revised June 11, 1976
NSG 7129

IMPACT EJECTA ON THE MOON*

JOHN D. O'KEEFE
DEPARTMENT OF GEOPHYSICS AND PLANETARY PHYSICS
UNIVERSITY OF CALIFORNIA
LOS ANGELES, CALIFORNIA

and

THOMAS J. AHRENS
SEISMOLOGICAL LABORATORY
CALIFORNIA INSTITUTE OF TECHNOLOGY
PASADENA, CALIFORNIA

*CONTRIBUTION NUMBER 2763, DIVISION OF GEOLOGICAL AND PLANETARY SCIENCES, CALIFORNIA INSTITUTE OF TECHNOLOGY, PASADENA, CALIFORNIA

Abstract

The partitioning of energy and the distribution of the resultant ejecta on the moon is numerically modeled using a Eulerian finite-difference grid. The impact of an iron meteoroid at 15 km/sec on a gabbroic anorthosite lunar crust is examined in detail. The high-speed impact-induced flow is described over the entire hydrodynamic regime from a time where the peak pressures are 6 Mbar until the stresses everywhere in the flow are linearly elastic, and less than 5 kbar. For 5-cm radius projectile the latter condition is achieved some $\sim$0.5 msec after impact. The effect of taking into account the shock-induced polymorphic phase changes, in the plagioclase and pyroxene structure (in gabbro) to the hollandite and perovskite structures, respectively, and the subsequent reversion to low-pressure phases is demonstrated to enhance shock-wave attenuation. A rate-dependent equation of state, is used for describing the hysteretic effect of the phase change. The ballistic equations for a spherical planet taking into account the decrease of gravity with height, are systematically applied to material with net velocity away from the moon. The mass of material escaping the moon corresponds to some 28% of the mass of meteorite, less than previous estimates, and most of the material lost, is lunar crust. Only 0.2% of the meteoroid escapes the moon, all in the vapor phase. In the case of accreting planets, a relatively sharp decrease in energy and mass lost from such impacts occurs when the escape velocities begin to exceed $\sim$1 km/sec. This implies that since the fraction of kinetic energy lost is less than 5%, impact heating of lunar-sized planets in the latter stages of accretion is efficient. Most of the impact energy remains on the lunar crust (86.1%) however the bulk of the impact energy (66.8%) resides in crustal impact

ejecta which is distributed with a surface density (mass/area) which decays as $R^{-2.715}$, where R, is the radius from the impact. At large distances from the impact, the ratio of lunar to meteorite ejecta is $\gtrsim 10^2$, implying that the higher concentrations of meteorite components observed in the Apollo 17 breccias, resulted from mostly local impacts.

INTRODUCTION

A central problem in describing the evolution of the terrestrial planets, especially in their later stages of accretion, is determining the partitioning of ejecta, in terms of mass and energy, upon impact of a meteorite. Although it is not yet clear whether the terrestrial planets formed from small particles in chemical and thermal equilibrium with the primordial gaseous nebulae as proposed by Lewis (1972), or from a chemically heterogeneous meteorite-like population of larger objects (Urey, 1952) or possibly, inhomogeneously directly from a condensing gas cloud (Clark et al., 1972), the present paper is concerned with how a lunar-sized object responds to the impact of meteoroids of $10^2 \lesssim$ km-radius. The present surface bears strong evidence that such meteoroids have impacted the moon since it evolved to approximately its present radius. Since some 80% of the highland samples returned from the lunar highlands are now known to be impact breccias with various stress and thermal histories, the thermal state and provenance of the ejecta from a single hypervelocity impact, needs to be studied in detail.

Recently, Overbeck et al. (1975) have argued that the ejecta from large impacts on the moon give rise to major transport and mixing processes which operated on both previous fragmental materials deposited on the moon (the regolith), as well as presumably the initial ejecta from the primary impact itself. The available evidence for such processes which may play an important role in modifying cratered surfaces, are based on photogeology and terrestrial cratering studies and subsequent theoretical analysis. This phenomena is not described in the present work, however.

Previously (O'Keefe and Ahrens, 1975, 1976) have examined in some detail the question of partitioning of energy from a large impact on the moon and

have, with assumptions regarding the properties of the meteorite and the lunar crust, calculated the decay, in space and time, of the strong shock which is induced by the impact. The shock is expected to alter the minerals of the crust as well as provide melted rock, unlike that resulting from normal igneous processes (Warner et al., 1973; Simonds, 1975).

Previous knowledge of ejecta distributions from hypervelocity impacts onto geologic materials is confined to photographic recording of the formation of the ejecta plume, transient cavity, and post-impact analyses of mass movement. Impact flows from mm-sized projectiles at speeds of 6-7 km/sec were studied. These experiments employed quartz sand (Braslau, 1970 and Stöffler et al., 1975) and solid basalt (Gault et al., 1963) target media and have provided considerable data on the general impact energy partitioning, and the shape and evolution of the ejecta plume. Although carried out under the earth's gravity field at pressures of 3 to 0.5 mm Hg, the quantitative post-impact ejecta distributions measured by Stöffler et al., have provided some experimental support for the relatively uncertain ejecta thickness distributions assumed by McGetchin et al. (1973) to infer thicknesses of basin deposits at the various Apollo landing sites. Although the quantity of meteoroid material in the present calculation is small, ($\sim$ 4 kg), and since we have not included gravity body forces in the cratering flow itself, we believe the results obtained in the large Froude number regime can be scaled to large impacts to the degree that the moon's curvature in the region of high-pressure flow can be neglected.

The objective of the present study is to examine the partitioning of impact energy, into the kinetic and internal energy of the ejecta, and to examine the spatial distribution of ejecta on the moon. The spatial

distribution of the meteorite debris and lunar-surface ejecta are separately treated. We also consider briefly the implications of this, initial, calculation on the larger question of accretionary processes for the terrestrial planets.

CALCULATIONAL OBJECTIVES

The present results were obtained by using the conservation of mass, momentum, and energy equations in finite-difference form (Hageman and Walsh, 1970) within a Eulerian framework with approximate equations-of-state as outlined previously (O'Keefe and Ahrens, 1975).

For this initial calculation it was assumed, that the meteorite had an iron-like composition because the appropriate equation-of-state is well known. Although differentiating the meteorite debris from lunar surface fragments in the calculation turns out not to be a problem, initially it presented conceptual difficulties. Unfortunately, an iron meteoroid in some respects, is probably atypical of objects which have impacted the moon, in light of the gross depletion of iron on, or within, the moon (compared to the other terrestrial planets). With this drawback in mind in the present calculation,the impact of an iron object is assumed at 15 km/sec. This velocity lies within an average range of from 15 to 18 km/sec inferred by Zook (1975) for the present moon and is similar to meteoroid velocities observed as radiant shows by the Prairie Network (Wassen, 1973, p. 137). Impact velocities on the order of at least $\sim$ 10 km/sec can, independently, also be inferred on the basis of the present knowledge of the Hugoniot curves for rocks, and the shock-metamorphic effects, especially melting, associated with rocks studied in-situ and within the ejecta, from many of the impact

craters found on the earth. The present calculation therefore deals with the ejecta from the flow produced by a 15 km/sec impact of an iron object on a gabbroic anorthosite half-space (in the vicinity of the impact, ~ 100 meteorite radii). However, once the initial ejecta velocity spectra are calculated, the ejecta paths are calculated for a spherical moon. The equation of state of the moon is modeled using data from sample 15,418 (Ahrens et al., 1973).

Two new features now incorporated in the calculation which should make the present work more credible and useful are:

(1) An explicit description of the kinetics of shock-induced phase changes for silicates comprising the lunar crust. This is provided by an algorithm which in essence prescribes a time-dependent equation-of-state. This brings the description of silicates into agreement with the release adiabat data, obtained in the mixed-phase regime reported by Ahrens et al. (1969), Petersen et al.(1970) and Grady et al. (1974).

(2) Inclusion of the necessary ballistic equations to calculate the trajectories of ejecta. Of specific interest are the mass and internal and kinetic energy content of both the initial ejecta which escapes the moon, or another terrestrial planet, as a function of escape velocity, as well as the spatial distribution of ejecta density at various times on a spherical moon.

EQUATIONS OF STATE

The shock wave data for plagioclase and pyroxene (McQueen et al., 1967; Ahrens et al., 1969; and Ahrens and Gaffney, 1972) demonstrate that both the component minerals, as well as rocks containing these minerals, undergo a

probable succession of shock-induced changes above ~ 125 to 150 kbars. The occurrence of these solid-solid transitions is not a trivial detail, since they account for ~ 35% increase in equivalent zero-pressure density. This results in almost an order of magnitude more compression, than the intrinsic self-compression of the minerals up to the transition pressure! Complete transformation to high-pressure phases is expected to occur in the 500 to 700 kbar range in a lunar crustal rock such as 15,418 (Ahrens et al., 1973). Coincidentally upon release of shock pressure from this pressure range the onset of melting occurs (De Carli and Milton, 1965 and Kieffer et al., 1976). Both the Hugoniot data and the results of static high-pressure phase studies demonstrate that the high-pressure phases most probably produced in the shock case for plagioclase is in the hollandite structure (Ahrens et al., 1969) and for pyroxene in the perovskite structure (Liu, 1975). The latter result was anticipated in interpreting the initial results for gabbroic anorthosite (Ahrens et al., 1973). Taking this into account, we have separately fitted an equation-of-state of the Tillotson form for each phase (O'Keefe and Ahrens, 1975). In the compressed region ($\rho > \rho_o$) the pressure is given by

$$P = \left\{ a + b/[E/(E_o\eta^2) + 1] \right\} E\rho + A\mu + B\mu^2 \qquad (1)$$

where P is pressure, ρ_o is the initial density, E specific internal energy, $\eta \equiv \rho/\rho_o$ and $\mu = \eta - 1$. Here (a + b) and, A, are the zero-pressure and low-temperature, Gruneisen parameter and bulk modulus, respectively. The constant, a, was taken to be 0.5 so that at high-energy densities the thermal pressure would approach that of an electron gas. For low densities and high temperatures, such that $\rho < \rho_o$ and with $E > E'_s$, the form used is:

$$P = aE\rho + \left\{ bE\rho/[E/E_o\eta^2) + 1] + A\mu\, e^{-\beta[V/V_o) - 1]} \right\} e^{-\alpha[V/V_o - 1]^2} \quad (2)$$

where α and β were chosen so that the equation approaches a polytropic equation-of-state at low densities and high specific internal energies with a polytropic exponent of $(a + 1)$.

In Table 1, the parameters for the high- and low-pressure phases (Fig. 1) are given, and E_s and E'_s represent the energy for incipient and complete vaporization at atmospheric pressure. In order to achieve unloading along isentropes which approximate those observed for feldspars by Ahrens et al. (1969) and Grady et al. (1975) above ~150 kbar, we have employed the phenomenological model of Horie (1966). The total energy and specific volume are given by

$$V = f_{eq}V_{hpp}(P,E) + (1-f_{eq})\, V_{\ell pp}(P,E) \quad (3)$$

$$E = f_{eq}E_{hpp}(P,E) + (1-f_{eq})\, E_{\ell pp}(V,E) \quad (4)$$

where the subscripts hpp and ℓpp indicate low- and high-pressure phases, and thermodynamic equilibrium in the mixed phase region is treated the same as in O'Keefe and Ahrens (1976). The time variation of the mass fraction, f, of material in the high-pressure phase is assumed to be given by

$$df/dt = (f_{eq} - f)/\tau \quad (5)$$

where f_{eq} is the equilibrium (minimum free-energy) mass fraction and τ is the time constant of reaction. As indicated in Table 1, the increase in internal energy upon transforming from the low- to high-pressure phase is taken as 0.013 Mbar-cm^3/g, independent of temperature. Based on the

experimental unloading profiles of Grady et al. (1974) for release data taken in the quartz-stishovite regime, τ, is assumed to be ~ 0.25 μsec.

It is worth commenting on the consistency of the constants of Table 1, based largely on Hugoniot data and Thomas-Fermi calculations, with other more conventional shock wave reductions of data, and the high-temperature, low-pressure properties. This can sensibly be done only in the case of iron, for which the present results predict incipient and complete melting to occur upon adiabatic release from principal Hugoniot states at ~ 0.63 and ~ 0.93 Mbar, respectively. Whereas, post-shock temperatures comparable to the melting point (1808°K) are calculated, to occur upon pressure release from ~ 1.7 Mbar (McQueen et al., 1970). Moreover the Tillotson formulation (Eq. 1.) overestimates the post-shock, complete-melt density at 7.39 g/cm^3, whereas, the measured density of liquid iron, at the melting point is ~ 7.00 to 7.01 g/cm^3. Finally, conventional Mie-Gruneisen reduction of the shock wave data predicts a post-shock density, which is too low, 6.704 g/cm^3, at the melting point (McQueen et al., 1970). We suspect some of these discrepancies may arise from a lack of properly taking into account the α-ε phase change and what is now known about the iron melting relations (Liu and Bassett, 1975).

Since the present high-speed flow calculations can be carried out to relatively long times at which point the stress field becomes linearly elastic, the yield criteria and complete elastic constants arising from an assumed Poisson's ratio of 0.20 must be utilized.

The finite-difference formulation permits a full tensorial treatment in cylindrical coordinates of stress and strain in the finite strength regime. A simple model which will account for dynamic yielding should, for example, specify the maximum shear-stress "or strength" supportable by the medium,

allow this strength to increase with increasing mean principal stress, and also account for the thermal weakening of the material by allowing the yield strength, Y, to decrease with increasing internal energy content at constant strain. Using the second stress invariant, $2Y^2$, as a measure of the yield strength, following the treament of Hageman and Walsh (1970), we assumed the following form for Y for gabbroic anorthosite:

$$Y(\text{kbar}) = (2.69 + 337.6\mu - 901\ \mu^2)\ (1 - E/E_m) \qquad (6)$$

where E_m is the internal energy density required for incipient melting under standard conditions. Thus, in the calculation when the second stress invariant exceeds $2Y^2$ all stresses are reduced proportionately so as not to exceed the yield strength specified by Eq. 6.

The above Mohr-Coulomb type yield condition is based on at present, a very limited set of data for the dynamic yielding of plagioclase- and pyroxene-bearing rock. At zero-confining stress. Eq. 6 satisfies the failure data of Kumar (1968) for one-dimensional stress loading of a terrestrial basalt at rates of $\sim 10^6$ kbar/sec and the Hugoniot-elastic-limit data of Ahrens et al. (1973) at loading rates of $\sim 10^{10}$ kbar/sec for lunar gabbroic anorthosite (sample 15,418). Finally, although the Mohr-Coulomb criterion is applied for dynamic yielding under compressive loading, we have utilized the value of 0.5 kbar for the dynamic tensile strength of gabbroic anorthosite. (This value is certain to be dependent on rock volatile content.) Although some data on dynamic tensile failure for rocks are available (Shockley et al., 1975) we suspect our description of the latter stages of crater excavation, and hence, ejecta distribution within several crater radii, are sensitive to this poorly constrained quantity.

THE EFFECT OF THE SHOCK-INDUCED PHASE CHANGE ON THE IMPACT FLOW

Since previous calculations of impacts in silicate material have used equation-of-state formulations which simply faired through both the high- and low-pressure portions of the Hugoniot (O'Keefe and Ahrens, 1975; Bjork, 1956; and Gault and Heitowit, 1963), it is interesting to examine the details of the early cratering flow which are affected by the shock-induced phase change in the silicate.

In the present calculations, a spherical iron meteoroid was assumed to impact a gabbroic anorthosite lunar surface at a velocity of 15 km/sec, this calculation is similar in many respects to that previously described (O'Keefe and Ahrens, 1975). However, previously the radius of the meteoroid was 23.2 km and in this calculation the radius is 5 cm. The size of impacting body was made relatively small, because we wish to include the phase change kinetics and also because of considerations of numerical viscosity. To obtain the necessary numerical resolution so as to examine phase change evolution in time and space, the time step which is a function of the sonic plus mass propagation time across a cell, must be much less than the characteristic phase transformation time (τ = 0.25 μsec). This criterion restricts the size of the impacting object for acceptable cell numbers ($\lesssim$ 3000) to radii less than ~10 cm. In addition, the numerical viscosity is less for smaller mesh spacing.

We want to emphasize that even though the present calculation is for a 5 cm-radius impacting body, these results can be scaled. This impact calculation is valid at early times (when the mean particle velocity is greater than the escape velocity from the crater being excavated) for all bodies

whose radii (r) are much greater than the sonic velocity (c) times the characteristic phase-change time ($r >> \tau c$); in other words, these bodies for which the shock propagation time across the body is much greater than the characteristic phase-change time. The flow field obtained in the present calculation can be scaled to that for a nominal Mare Imbrium-type impact described by O'Keefe and Ahrens (1975) in which a 23.2 km-radius iron projectile is assumed as the impactor. The distance and time are scaled (hydrodynamically) using the ratio of projectile radii, $r_1/r_2 = 4.64 \times 10^5$. Thus for a time, $t_2 = 25.4$ μsec, for the present problem, the equivalent time in the initial report of (O'Keefe and Ahrens, 1975) is ~ 11.8 sec. The flow fields associated with both calculations, having a similar peak pressure, are compared in Fig. 2 and 3 and some key parameters of the two flows are listed in Table 2. In both flow fields the peak pressure is ~ 0.66 Mbar, however, the maximum depth of penetration of the meteorite without a phase change is 65 km compared to 54 km with a phase change. The most significant difference between the two flows is the rapid attenuation of shock pressure when the phase change is taken into account. This is demonstrated in Table 2. In our earlier calculation, the peak pressure extends to a depth of 118 km versus 66 km for the present case. The rapid attenuation results from the high rarefaction-wave velocity associated with the high-pressure phase material. Earlier, at this stage in the flow, (Fig. 2) the meteorite lay completely below the initial lunar surface, whereas in Fig. 3 a portion of the vaporized iron object is 5 km above the initial surface. Moreover, comparison of Figs. 2d and 3d demonstrates that much of this vaporized meteorite material is moving inward when phase changes are taken into account, whereas before the entire flow is still radially outward

at this time.

EJECTA BALLISTICS

At a series of times, in the present calculation, we have employed the ballistic equations for describing ejecta for which the net particle velocity of the flow is pointed above the local, flat, horizon. Taking the sphericity of the moon, and the decrease in gravity with height into account, yields for the range (Thomson, 1963

$$R = 2R_o \tan^{-1}\left\{\frac{\bar{V}_o^2 \sin\beta\cos\beta}{(1-\bar{V}_o^2\cos^2\beta)}\right\} \tag{7}$$

where

$$\bar{V}_o^2 = 2V_o^2/R_o g_o \tag{8}$$

Here R_o is the mean lunar radius, 1738 km, V_o is the magnitude of the velocity vector of the contents of a eulerian cell, g_o the surface gravitational acceleration, 161.8 cm/sec^2, and β is the elevation angle of the particle, from the local horizontal.

EJECTA AND PLANETARY ACCRETION

The relative amount of mass exceeding various escape velocities as a function of time is shown in Figure 4 for times early in the flow. It is significant that the amount of mass exceeding the escape velocity of the moon is approximately 20 percent of the mass of meteoroid.

At a much later time, 545 μsec, the amount of rock escaping the moon has increased only slightly, $\sim$ 28% of the mass of the meteoroid, however,

only ~ 2% of the escaping lunar material is vaporized as a result of the impact. Most of the meteoroid remains on the moon, our present calculations indicate, only 0.2% escapes, all in the vapor phase.

The present amount of material escaping the moon is less than would be predicted from the results of Gault et al. (1963) which are based on experiments with aluminum projectiles having diameters less than 3 mm. Moreover, they infer on the basis of high-speed framing camera photography that for impacts of 6.1 to 6.4 km/sec on the order of an equivalent mass of the projectile, probably largely target derived material, is ejected at speeds greater than the lunar escape velocity. Note that in the present calculations the mass exceeding the escape velocity of the moon reached its final value early in the impact flow (within 5 μsec, or in terms of larger-scale events, a time interval corresponding to translation of the meteoroid through a distance about equal to its radius). However, the amount of mass exceeding lower escape velocities, e.g., velocities less than ~ 1 km/sec, is still increasing at the end of 25 μsec. Referring to Fig. 5, the material exceeding an escape velocity of 1 km/sec is primarily in the liquid and vapor state, whereas the material having escape velocities less than 1 km/sec is primarily in the solid state, and the amount in the solid state is still increasing at the end of 25 μsec. One interesting feature of this figure is the sharp cutoff in mass lost at escape velocities slightly exceeding 1 km/sec. The implication is that for 15 km/sec meteoroids, the moon and larger bodies are efficient accretors, whereas for smaller bodies having escape velocities much less than a kilometer per second, the amount of mass lost exceeds the mass of the impacting meteoroid. The relative amount of energy lost as a function of escape velocity is shown in Figure 6. For impacts on bodies having

escape velocities greater than 1 km/sec, the fraction of energy lost is less than 5% and therefore impact heating of terrestrial planets in the latter stages of accretion is an efficient process.

Finally, we have examined the ejecta distribution at late times ($\sim$ 545 μsec), both to provide a first-order determination of crater volume, and secondly, to examine the ejecta blanket height versus radius in light of both the small-scale laboratory results, and the explosive data which have already been applied to the moon by McGetchin et al. (1972). The mass-flux distribution as a function of angle of ejection and velocity weighted by mass versus angle of ejection are shown in Figs. 7 and 8. This calculation is again for a 5-cm radius iron projectile (4 kg), impacting the moon at 15 km/sec. The shock pressures present in the impact-induced flow range from nearly 2 Mbar, at 9 μsec to $\sim$ 5 kbar, at 545 μsec. The ejecta plume is undoubtedly rather smooth versus the irregular pattern calculated, which demonstrates the effects of finite-sized zones. Even with 167 cells used to describe the meteorite at initial impact, the zoning used is too coarse to resolve the jetting which is known to occur under oblique conditions (Kieffer, 1975). The mass-weighted velocity versus angle plotted in Fig. 8, is effectively a plot of momentum distribution, in that the quantity summed per each 10° increment of angle is

$$\bar{m} = \sum_i V_{oi}\, m_i \Big| \sum_i m_i \qquad (9)$$

where V_o has the same meaning as in Eq. 8 and the summation is carried out over all particles with a net axial velocity away from the lunar surface. Note that taken together, Figs. 4, 7, and 8, indicate that while high-shock pressures are present in the flow, e.g. at 9 μsec, the mass of ejecta

present is of the order of the mass of the meteoroid and has a velocity on the order of $\sim 10^5$ cm/sec. (This is the only period during the cratering process in which material is lost from a moon of present size.) Moreover, at successively later times, as the mean pressure decays, so does the mass-weighted velocity and the ejecta achieves a mass-weighted velocity which is of the order of $\sim 10^2$ to 10^3 cm/sec. We suspect that the curves shown for 462 and 545 μsec, are dependent on the dynamic tensile criterion used in the calculation.

Comparison of the present ejecta patterns with small-scale laboratory experiments, largely carried out at impact exceeds significantly lower than those required to produce substantial vapor (Ahrens and O'Keefe, 1972) present some interesting contrasts. It should immediately be recognized that the expansion of the inner ejecta plume of vaporized meteorite depicted in Fig. 3 will give rise to late-time ejecta which have no counterpart in the experiments of Gault et al. 1963; Oberbeck and Morrison, 1976; and Schneider, 1975. Hence comparison with these results should involve ejecta distributions at relatively early times, i.e., 9 and 47 μsec, when the interacting shock and rarefaction wave effectively launch largely material from near the target free-surface. Comparison of Figs. 7 and 8 indicate that/at/early times the bulk of the low-speed ejecta is launched at low angles, whereas the higher speed ejecta (which is also hottest) is launched at higher angles. Qualitatively this is observed by Overbeck and Morrison in their shock launched ejecta. In our Eulerian calculation the entire flow field is in motion by the time the stresses are low, we cannot determine the initial position of each mass particle in the flow. It is interesting to note that the present ejecta flux is far more evenly distributed with respect elevation than would

be inferred from Gault et al. 1963 framing sequences. Like Gault et al. 1963 and McDonnel et al.1976 (both experiments carried out on crystalline silicates) and unlike the results of Schneider 1975 (carried out on a glass), the calculated ejecta flux is a maximum (at $\gtrsim 47$ μsec) at high elevation angles. It is also interesting that our calculation qualitatively gives an ejecta flux distribution with elevation having a broad minimum at $\sim 45°$ which resembles that of McDonnell et al. However, probably because of the gross velocity differences and rock strength and surface effects the relative amount of ejecta in our calculation is $\sim 2 \times 10^3$ greater.

We note that at late times (545 μsec) the total ejecta is about 1.6×10^8 grams for a meteorite having an initial mass of 4.079 kg. Thus the total amount of ejecta is about 4×10^5 times the mass of the meteorite. If a mean density of $2.7 g/cm^3$ for lunar crust and a crater depth-to-radius ratio of 0.4 is assumed for a conical shaped crater, an equivalent radius of 521 cm crater is calculated. This is plotted for comparison with terrestrial and lunar craters in Fig. 9. Our theoretical crater is seen to be similar in size to those mapped by Moore (1976) and perhaps most comparable to the Ranger craters produced by slower, but more massive projectiles impacting the more distended regolith. The present calculation gives the final mass of ejected meteorite as ~ 1500 grams, or one third of its initial mass. This value is again probably heavily affected by the rheology assumed for the meteoroid. A fluid was assumed for the present case.

Table 3 summarizes the partitioning of energy at late times (545 μsec). Of special interest is the great efficiency of the impact process in transferring kinetic energy into the thermal energy at the later stages of planetary accretion. As can be seen from the Table most of this thermal

energy resides in the lunar-surface ejecta which is spread over the moon in accordance with the distribution shown in Fig. 10. The ejecta that travels the farthest is the initial ejecta. This is also the hottest. Since the stresses at late times have all decayed into the assumed elastic range, the present calculation implies that little of the kinetic energy, 1.1% of the projectile energy resides in the non-ejecta component. The 1.1% value, then represents energy which ultimately will largely remain as internal energy in the vicinity of the impact as only ~ 0.01 to 0.1% of the impact energy is inferred to convert to seismic energy (Schultz and Gault, 1975).

The ejecta distributions for meteoroid fragments and lunar surface ejecta for early and late times are shown in Fig. 10. These are obtained using the trajectory of the contents of each cell moving away from the lunar surface. At 545 μsec there are some 123 cells of variable mass in such trajectories, each with a mean internal energy. The ejecta surface density is calculated by determining the end point of each trajectory on a spherical moon.

At late times at distances, $\gtrsim 10^4$ cm from the impact, the calculated ejecta surface density, Λ, on a spherical moon can be fit with

$$\Lambda(g/cm^2) = 1.29 \times 10^9 \, R^{-2.715} \tag{10}$$

where R(cm) has the same meaning as in Eq. 7. Subdividing the ejecta distribution into close-in, and far-out, regimes is clearly arbitrary, since the first-three shortest radii surface densities calculated, lie within the hypothetical crater. At late times the meteorite ejecta, which is very coarsely zoned (i.e. only three particles!), can be fit with

$$\Lambda(g/cm^2) = 4.42 \times 10^7 \, R^{-2.930} \tag{11}$$

These observed ejecta densities decay with radii slightly less rapidly than the observations made on a half space, at low atmospheric pressures, for sand, in the earth's gravity field by Stöffler et al. They observed a decay of $R^{-3.26}$. McGetchin et al. assumed a value of $R^{-3.0}$ for estimating thicknesses of basin deposits on a flat moon. The ratio, T, of lunar rock ejecta to meteorite ejecta is $\gtrsim 10^2$. This ratio, to first order, should be independent of projectile size since the ranges calculated are independent of projectile mass. The present values for T are somewhat greater than the values inferred for Apollo 17 breccias by Morgan et al. (1974). Taking the Morgan et al data and the calculated radius dependence for T at face value implies that if the siderophile minor element contents measured in the Apollo 17 breccia boulders come from tne one projectile, and different breccia samples have geochemical imprints of different objects, the impact events occured at ranges where $T \leq 10^2$, or at $R \lesssim 1$ km, from the Apollo 17 site and hence do not represent the major basin forming impacts.

ACKNOWLEDGMENTS

This research was supported by NASA Grant (NSG 7129). We appreciate the computational assistance of M. Lainhart. The critical comments made by F. Horz, H. Moore and D. E. Gault on this paper were most helpful.

REFERENCES

Ahrens, T. J., and Gaffney, E. S. (1971) Dynamic compression of enstatite. J. Geophys. Res. 76, 5504-5513.

Ahrens, T. J., and O'Keefe, J. D. (1972) Shock melting and vaporization of lunar rocks and minerals. The Moon 4, 214-249.

Ahrens, T. J., O'Keefe, J. D., and Gibbons, R. V. (1973) Shock compression of a recrystallized anorthositic rock from Apollo 15. (Suppl. 4) Geochimica et Cosmochimica Acta 3, 2575-2590.

Ahrens, T. J., Peterson, C. F., and Rosenberg, J. T. (1969) Shock compression of feldspars. J. Geophys. Res. 74, 2727-2746.

Bjork, R. L. (1961) Analysis of the formation of Meteor Crater, Arizona: A preliminary report. J. Geophys. Res. 66, 3379-3388.

Breslau, D. (1970) Partitioning of energy in hypervelocity impact against loose sand targets. J. Geophys. Res. 75, 3987-3999.

Clark, S. P., Turekian, K. K., and Grossman, Lawrence (1972) Model for the early history of the earth, in The Nature of the Solid Earth, E. C. Robertson, ed., McGraw Hill, Inc., pp. 19-40.

Fechtig, H., Hartung, J. B. Nagel, K., and Neukum, G. (1974) Lunar microcrater studies, derived meteoroid fluxes, and comparison with satellite-borne experiments. Proc. 5th Lunar Sci. Conf. (Suppl. 5) Geochimica et Cosmochimica Acta 3, 2463-2474.

Gault, D. E. (1973) Displaced mass, depth, diameter, and effects of oblique trajectories for impact craters formed in dense crystalline rocks. The Moon 6, 32-44.

Gault, D. E., and Heitowit, E. D. (1963) The partition of energy for hypervelocity impact craters formed in rock. Proc. Sixth Hypervelocity Impact Symposium 2, 219-456 Cleveland, Ohio (unpublished).

Gault, D. E., Shoemaker, E. M., and Moore H. J. (1963) Spray ejected from the lunar surface by meteoroid impact. NASA, Technical Note D-1767, pp. 39.

Grady, D. E., Murri, W. J., and Fowles, G. R. (1974) Quartz to stishovite: Wave propagation in the mixed phase region. J. Geophys. Res., 79, pp. 332-338.

Grady, D. E., Murri, W. J., and De Carli, P. S. (1975) Hugoniot sound velocities and phase transformation in two silicates. J. Geophys. Res. 80, 4857-4861.

Hageman, L. J., and Walsh, J. M. (1970) Help, a multimaterial eulerian program for compressible fluid and elastic-plastic flows in two space dimensions and time. Systems, Science, and Software Report, 3SR-350, Vol. 1.

Horie, Y. (1966) The kinetics of phase change in solids by shock compression. Washington State University Ph.D. Thesis.

Kieffer, S. W. (1975) Droplet chondrules. Science, 189, 333-340.

Kieffer, S. W., Schaal, R. B., Gibbons, R., Hörz, F., Miltin, D. J., and Dube, A. (1976) Shocked basalts from Lunar Impact Crater (India) and experimental analogues. Proc. Lunar Sci. Conf. 7th, (in press).

Kumar, A. (1968) The effect of stress rate and temperature on the strength of basalt and granite. Geophysics 33, 501-510.

Lewis, J. S., (1972) Metal/silicate fractionation in the solar system. Earth and Planet. Sci. Letters 15, 286-290.

Liu, L., and Bassett, W. A. (1975) The melting of the iron up to 200 kbar. J. Geophys. Res. 80, 3777-3782.

Liu, L. (1975) Post-oxide phases of olivine and pyroxene and mineralogy of the mantle. Nature 258, 510-512.

McDonnell, J. A., Flavill, R. P., and Carey, W. C. (1976) Microparticle hypervelocity impact communication distributions, primary crater and accretionary populations on lunar samples (abstract). In Lunar Science VII, 521-523. The Lunar Science Institute, Houston.

McGetchin, T. R. Settle, M., and Head, J. W. (1973) Radial thickness variation in impact crater ejecta: Implication for lunar basin deposits. Earth and Planet. Sci. Letters 20, 226-236.

McQueen, R. G., March, S. P., Fritz, J. N., (1967) Hugoniot equation of state of twelve rocks. J. Geophys. Res. 72, 4999-5036.

McQueen, R. G., Marsh, S. P., Taylor, J. W., Fritz, J. N., and Carter, W. J., (1970) The equation of state of solids from shock wave studies. In High Velocity Impact Phenomena, ed. by R. Kinslow, Academic Press, 294-416.

Milton, D. J., and De Carli, P. S. (1963) Maskelynite: formation by explosive shock. Science 140, 670-671.

Moore, H. J. (1976) Missile impact craters, (White Sands Missile Range, New Mexico) and applications to lunar research, U.S.G.S. Professional Paper, 812-B.

Morgan, J. W., Ganapathy, R., Higuchi, H., Krahenbuhl, V., and Anders, E. (1974) Lunar basins: Tentative characterization of projectiles, from meteoritic elements in Apollo 17 boulders. Proc. Lunar Sci. Conf. 5th 1703-1736.

Oberbeck, V. R., and Morrison, R. H. (1976) Effect of basin secondaries and debris surges on survival of post accretional lunar and planetary surfaces (abstract). In Lunar Science VII, 642-644. The Lunar Science Institute, Houston.

Oberbeck, V. R., Morrison, R. H., and Hörz, F., (1975) Transport and emplacement of crater and basin deposits, The Moon 13, 9-26.

O'Keefe, J. D., and Ahrens, T. J. (1975) Shock effects from a large impact on the moon. Proc. Lunar Sci. Conf. 6th, p. 2831-2844.

O'Keefe, J. D., and Ahrens, T. J. (1976) Impact flows and crater scaling on the moon, Proc. Roy. Soc. Disc. Mtg. on the Moon, Phil. Trans. Roy. Soc. of London (in press).

Petersen, C. F., Murri, W. J., and Cowperthwaite, M. (1970) Hugoniot and release-adiabat measurements for selected geologic materials. J. Geophys. Res. 75, 2063-2072.

Schneider, E. (1975) Impact ejecta exceeding lunar escape velocity. The Moon 13, 173-184.

Schultz, P. H., and Gault, D. E. (1975) Seismically induced modification of lunar surface features. Proc. Lunar Sci. Conf. 6th, p. 2845-2862.

Shockley, D. A., Petersen, C. F., Curran, D. F., and Rosenberg, J. T. (1972) Dynamic tensile failure in rocks, Annual Report. Stanford Research Institute Report, PYU-1087, 70.

Simonds, C. H. (1975) Thermal regimes in impact melts and the petrology of the Apollo 17 Station 6 boulder. Proc. Lunar Sci. Conf. 6th, 641-672.

Stöffler, D., Gault, D. E. Wedekind, J. and Polkowski, G., (1975) Experimental hypervelocity impact into quartz sand: Distribution and shock metamorphism of ejecta. J. Geophys. Res. 80, 4062-4077.

Tillotson, J. H. (1962) Metallic equations of state for hypervelocity impact. General Atomic Report GA 3216.

Thomson, W. T. (1963) Introduction to Space Dynamics, John Wiley.

Urey, H. C. (1952) The Planets, Yale University Press.

Warner, J. L., Simonds, C. H., and Phinney, W. C., Apollo 16 rocks: Classification and petrogenetic model, Proc. Lunar Sci. Conf. 4th, 481-504.

Wasson, J. T. (1974) Meteorites, Springer-Verlag, pp. 316.

Zook, H. A. (1975) The state of meteoritic material on the moon. Proc. Lunar Sci. Conf. 6th, 1653-1672.

Table 1. Equation of State Parameters

Material	ρ_o (g/cm^3)	a	b	A (Mb)	B (Mb)	E_o Mb-cm^3/g	E_s Mb-cm^3/g	E_s' Mb-cm^3/g	α	β
Gabbroic Anorthosite										
lpp[1]	2.936	0.5	0.107	0.705	1.34	9.099	0.030	0.170	5.0	5.0
hpp[2,3]	3.965	0.5	0.429	2.198	1.01	0.906	0.030	0.170	5.0	5.0
Iron[4]	7.8	0.5	1.5	1.28	1.05	0.095	0.0244	0.102	5.0	5.0

(1) Fit to experimental data on Sample 15,418 and Thomas-Fermi calculations.

(2) Fit to Hugonoit data derived from elastic constant systematics and Thomas-Fermi calculations.

(3) Two phase regime parameters: E_T^* = 0.01323 (Mb-cm^3/g), ρ_{lpp} = 3.42 (g/cm^3). ρ_{hpp} = 4.18 (g/cm^3)

(4) Tillotson (1962).

*E_T is the transition energy between the lpp and hpp phases.

Table 2

Comparison of impact flow fields for 23.2 km radius, 15 km/s iron meteoroid at 9.35 sec no phase change (Fig. 2) as compared to flow for phase change in gabbroic anorthosite (Fig. 3) 25.4 μsec after impact, distance scaled to 23.2 km-radius impacting object.

Parameter	Units	Fig. 2 (no phase change)	Fig. 3 (phase change)
Min. depth meteorite	km	23	-3
Max. depth meteorite	km	65	54
Max. diameter deformed meteorite	km	115	103.5
Peak pressure	Mbar	0.662	0.66
Depth from surface to 1% peak pressure along centerline	km	56	47
Depth from surface to 50% peak pressure along centerline	km	100	53
Depth to 100% peak pressure along centerline	km	118	66
Peak pressure, meteorite-moon interface	Mbar	0.041	0.396
Max. depth of shock along centerline (1% peak pressure on leading edge)	km	140	75

Table 3. Gross Energy Partitioning for 15 km/sec

Impact of Iron Object onto Gabbroic Anorthosite

	Kinetic Energy	Internal Energy	Total
	(%)	(%)	(%)
Lunar Surface	6.9	86.1	93.0
(ejecta)*	(5.8)	(66.8)	
Iron Object	0.0205	6.7	6.7
(ejecta)	(.0062)	(2.4)	

* Indicated by parenthesis

Figure Captions

Figure 1. Equation of state of gabbroic anorthosite in low (ℓpp) and high pressure (hpp) regimes. Log_{10} (pressure) versus compression . The pressure range assumed for mixed-phase regime is indicated. Equation of state of 2.86 g/cm^3 basalt used in Gault and Heitowit (1963) (G & H) formulation is shown also for comparison. In the G & H treatment release adiabats are assumed to coincide with Hugoniot curve.

Figure 2. Hypervelocity flow field for 23.2 km radius, 15 km/sec iron meteorite striking a gabbroic anorthosite lunar crust, 9.35 sec after impact (scale time for 5-cm radius meteoroid is 20.2 μsec). Phase changes <u>have not</u> been specifically taken into account. Contour values give percentage of difference between minimum (min) and maximum (max) value (cgs) indicated for each variable. (a) pressure, min = -2.25×10^9, max = 6.62×10^{12}; (b) internal energy, min = 0.0, max = 1.81×10^{11}; (c) axial velocity, min = -2.47×10^5, max = 5.35×10^5; and (d) radial velocity, min = 0.0, max = 2.81×10^5, after O'Keefe and Ahrens (1975). Vertical and horizontal scales are identical.

Figure 3. Hypervelocity flow field for 5-cm radius, 15 km/sec iron meteorite striking a gabbroic anorthosite lunar crust, 25.4 μsec after impact. Second scale shown is that appropriate for comparison to 23.2 km radius meteorite impact of Fig. 2. Phase changes have been taken into account. Contour values give percentage of difference between minimum (min) and maximum (max) value (cgs) indicated for each variable. (a) pressure, min = -2.0×10^7, max = 6.6×10^{11};

(b) internal energy, min = -1.3×10^{10}, max, = 1.2×10^{11};

(c) axial velocity, min = -2.7×10^{5}, max = 6.5×10^{5}; and

(d) radial velocity, min = -1.9×10^{5}, max = 2.4×10^{5}.

Figure 4. Relative mass escaping planetary gravity field as a function of time and escape velocity for 15 km/sec iron meteoroid impacting gabbroic anorthosite crust.

Figure 5. Lower bound of relative mass partitioned in terms of vapor, liquid, and solid escaping planet from 15 km/sec iron meteoroid impact as a function of escape velocity at a characteristic time of 25 μsec for a 5-cm radius meteoroid.

Figure 6. Lower bound of relative energy (partioned in terms of that contained in vapor, liquid and solid ejecta) escaping planet from 15 km/sec iron meteoroid impact as a function of escape velocity at a characteristic time of 25 μsec for 5-cm radius meteoroid.

Figure 7. Ejected mass flux versus ejection angle from lunar surface at various times. Flow corresponds to a 5-cm radius projectile striking a gabbroic anorthosite target initially at 15 km/sec.

Figure 8. Mass weighted, ejecta velocity versus ejection angle from lunar surface at various times. (Same flow as in Fig. 7.)

Figure 9. Log_{10} (crater radius) versus Log_{10} (total estimated impact energy), for various laboratory (Gault, 1973; Fechtig et al. 1974) and field observations (Moore, 1976, also see O'Keefe and Ahrens, 1976). Large symbol indicates theoretical crater radius calculated for ejecta mass calculated for 5-cm iron projectile impacting gabbroic anorthosite at 15 km/sec.

Minimum gravitational energy line calculated for bowl-shaped crater for, 3 g/cm^3 density rock using formulae of O'Keefe and Ahrens, 1976.

Figure 10. Ejecta density on the moon versus range from center of crater. Large symbols are ejecta distribution at 545 μsec after impact of 15 km/sec, iron meteorite into gabbroic anorthosite. Small symbols are distribution of initial, hot, ejecta calculated from particle trajectories 25 μsec after impact.

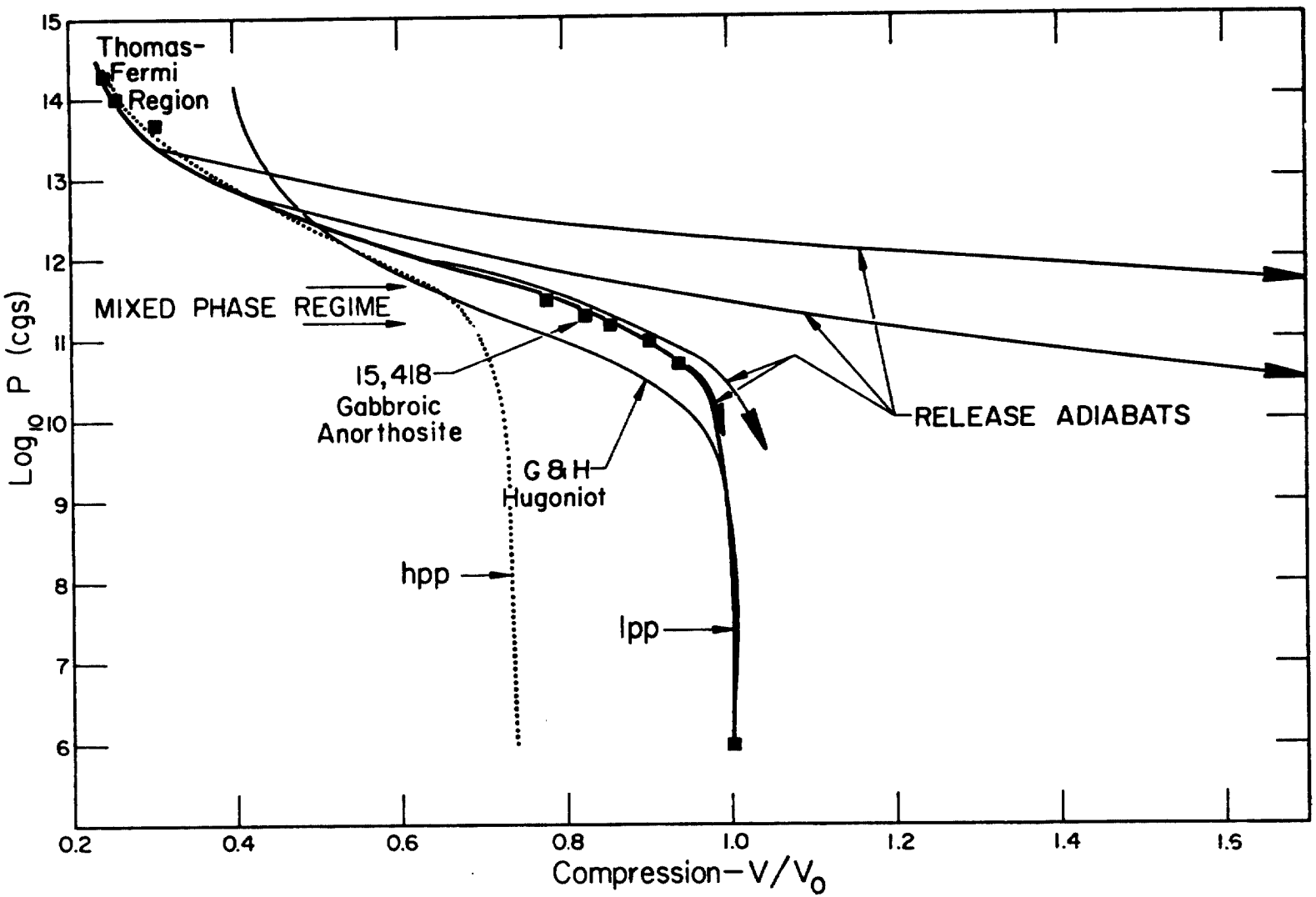
Thomas-
Fermi
Region
MIXED PHASE REGIME
15,418
Gabbroic
Anorthosite
G & H
Hugoniot
hpp
lpp
RELEASE ADIABATS
Log10 P (cgs)
Compression – V/V0
15
14
13
12
11
10
9
8
7
6
0.2
0.4
0.6
0.8
1.0
1.2
1.4
1.6

Fig. 1

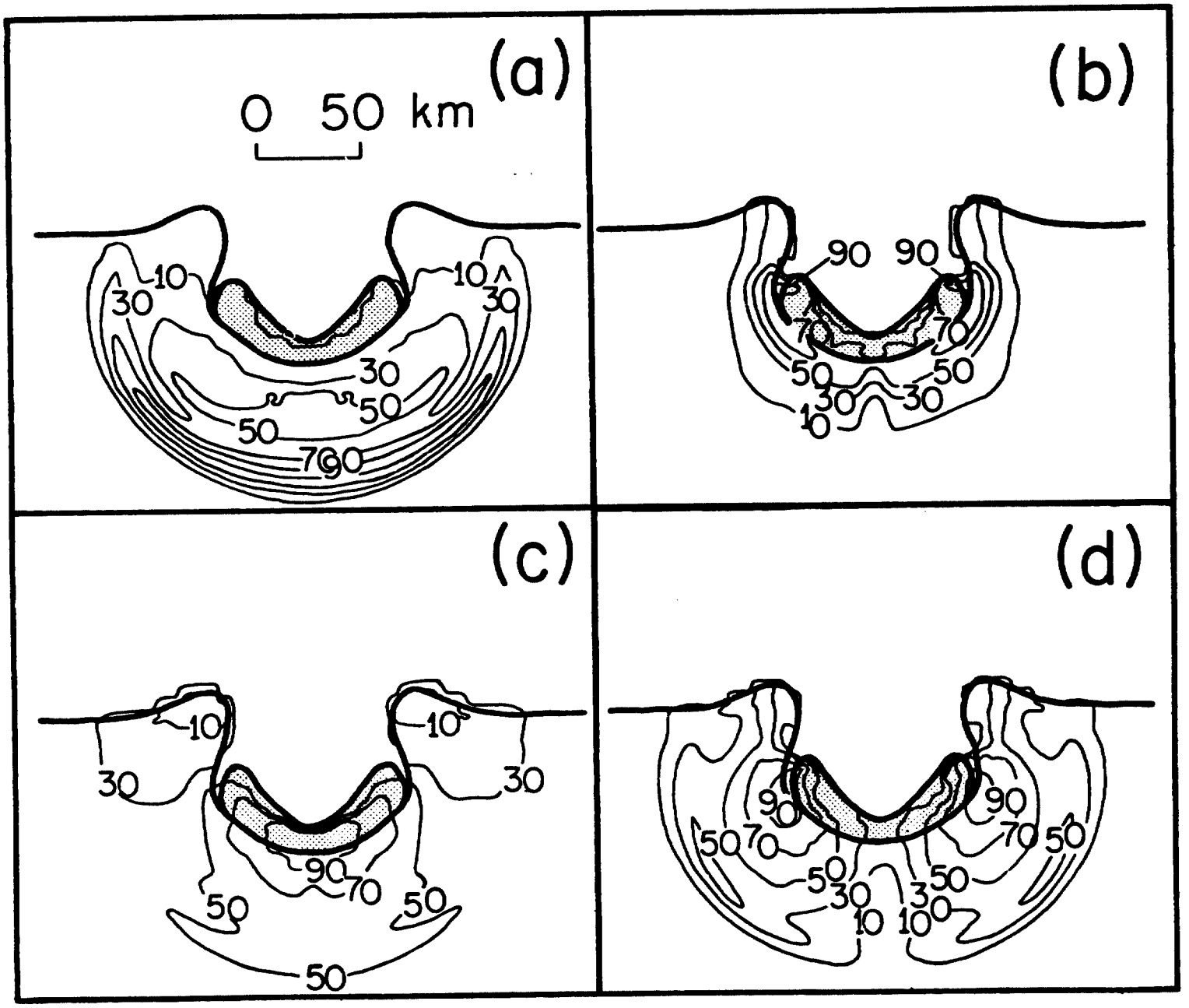
(a)
0 50 km
10
30
10
30
30
50
50
70
90
(b)
90
90
70
70
50
50
30
30
10
(c)
10
10
30
30
90
70
50
50
50
(d)
90
90
50
70
70
50
50
30
50
30
10
10

Fig. 2

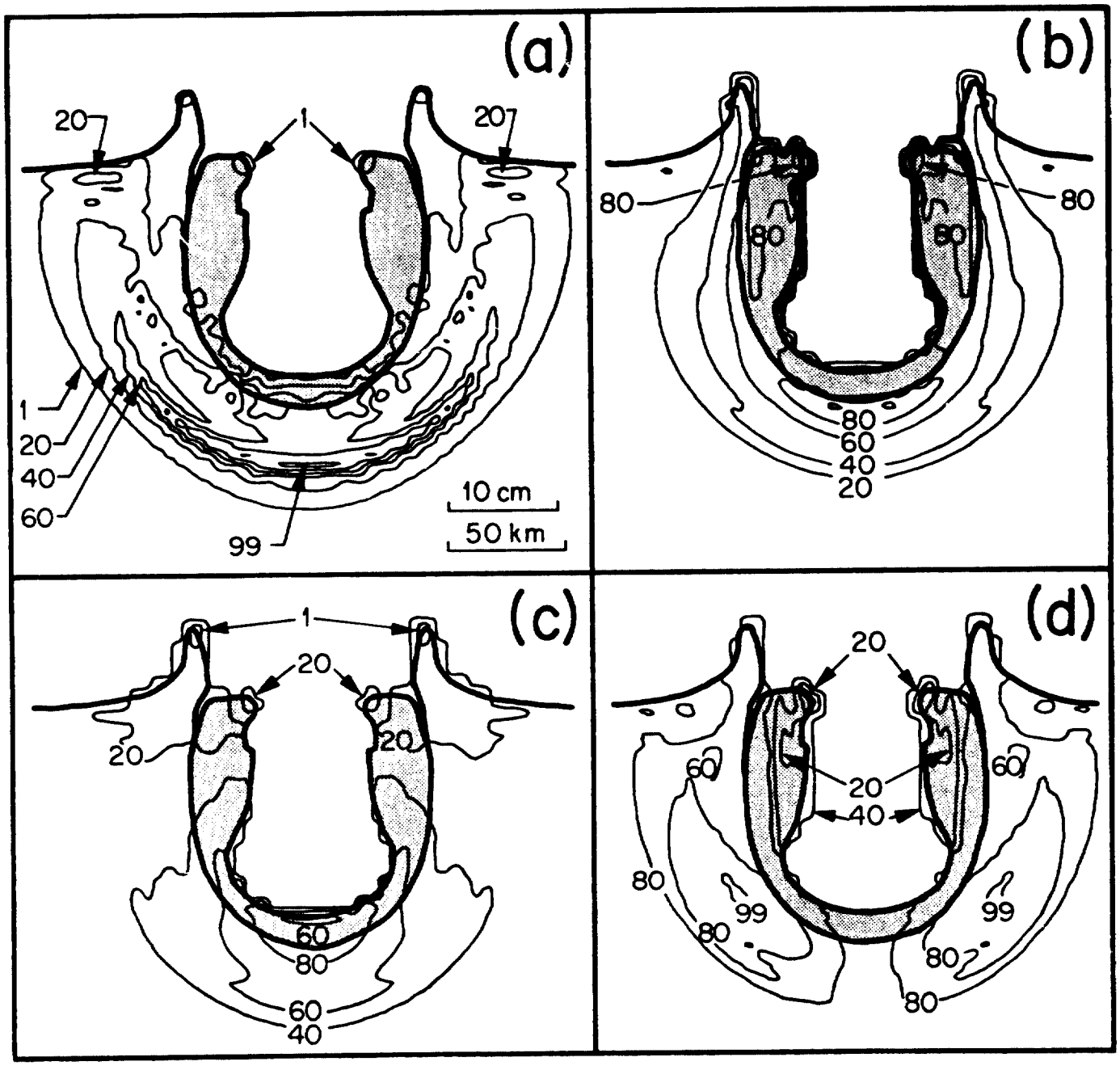
(a)
20
1
20
1
20
40
60
99
10 cm
50 km
(b)
80
80
80
80
60
40
20
(c)
1
20
20
20
60
80
60
40
(d)
20
60
60
20
40
80
99
80
99
80
80

Fig. 3

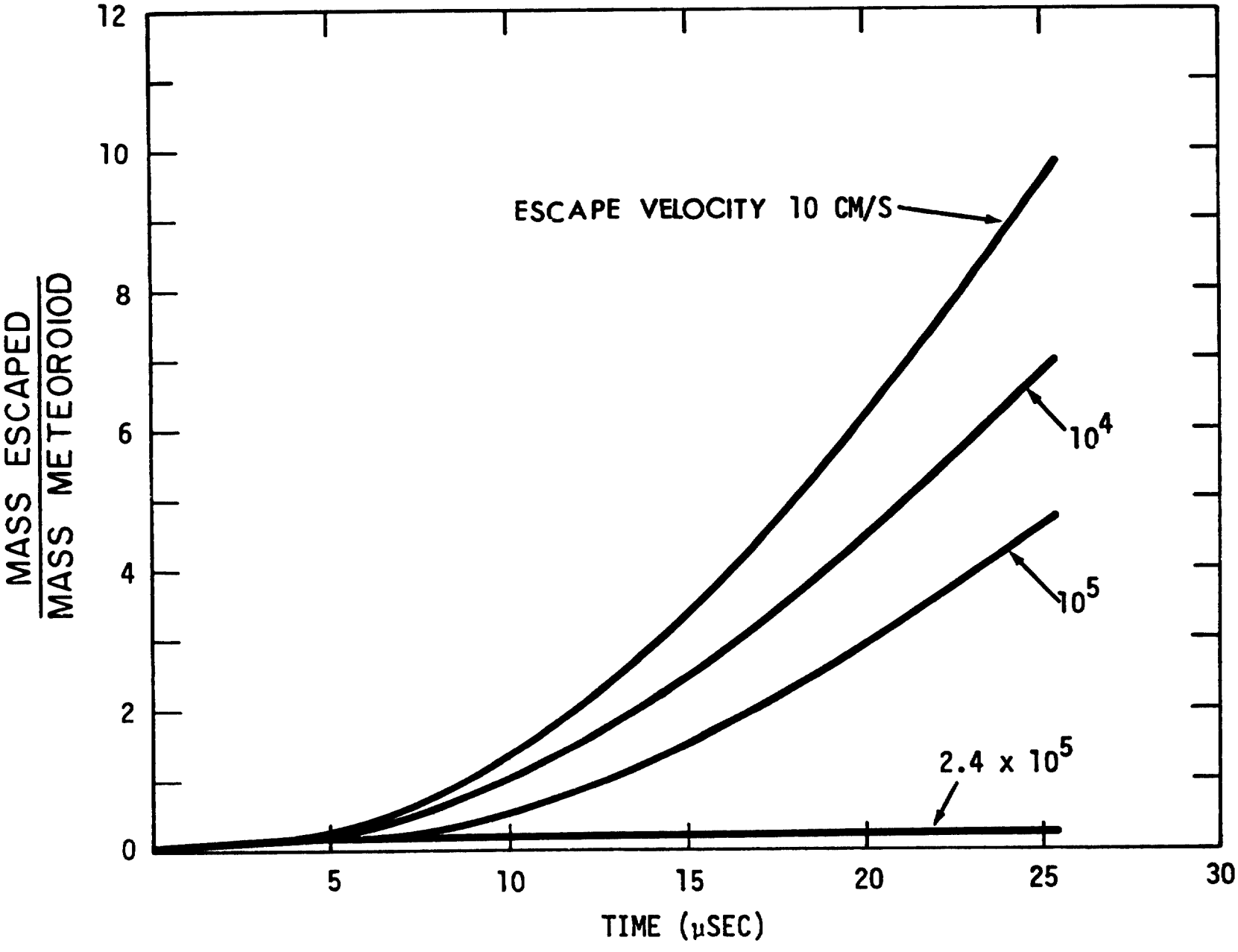
12
10
8
6
4
2
0
MASS ESCAPED / MASS METEOROIOD
ESCAPE VELOCITY 10 CM/S
10^4
10^5
2.4×10^5
5
10
15
20
25
30
TIME (μSEC)

Fig. 4

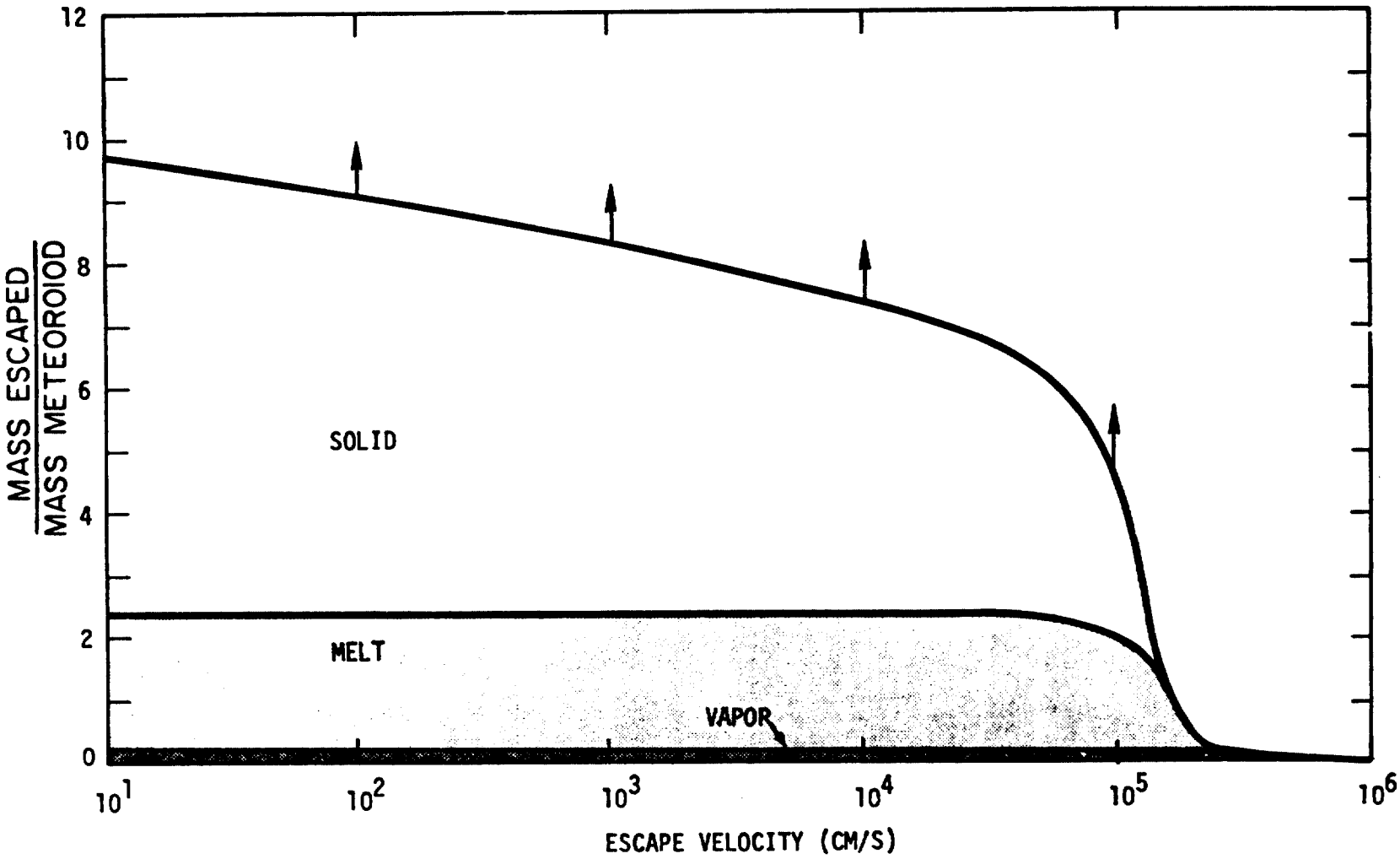
12
10
8
6
4
2
0
MASS ESCAPED / MASS METEOROIOD
SOLID
MELT
VAPOR
10^1
10^2
10^3
10^4
10^5
10^6
ESCAPE VELOCITY (CM/S)

Fig. 5

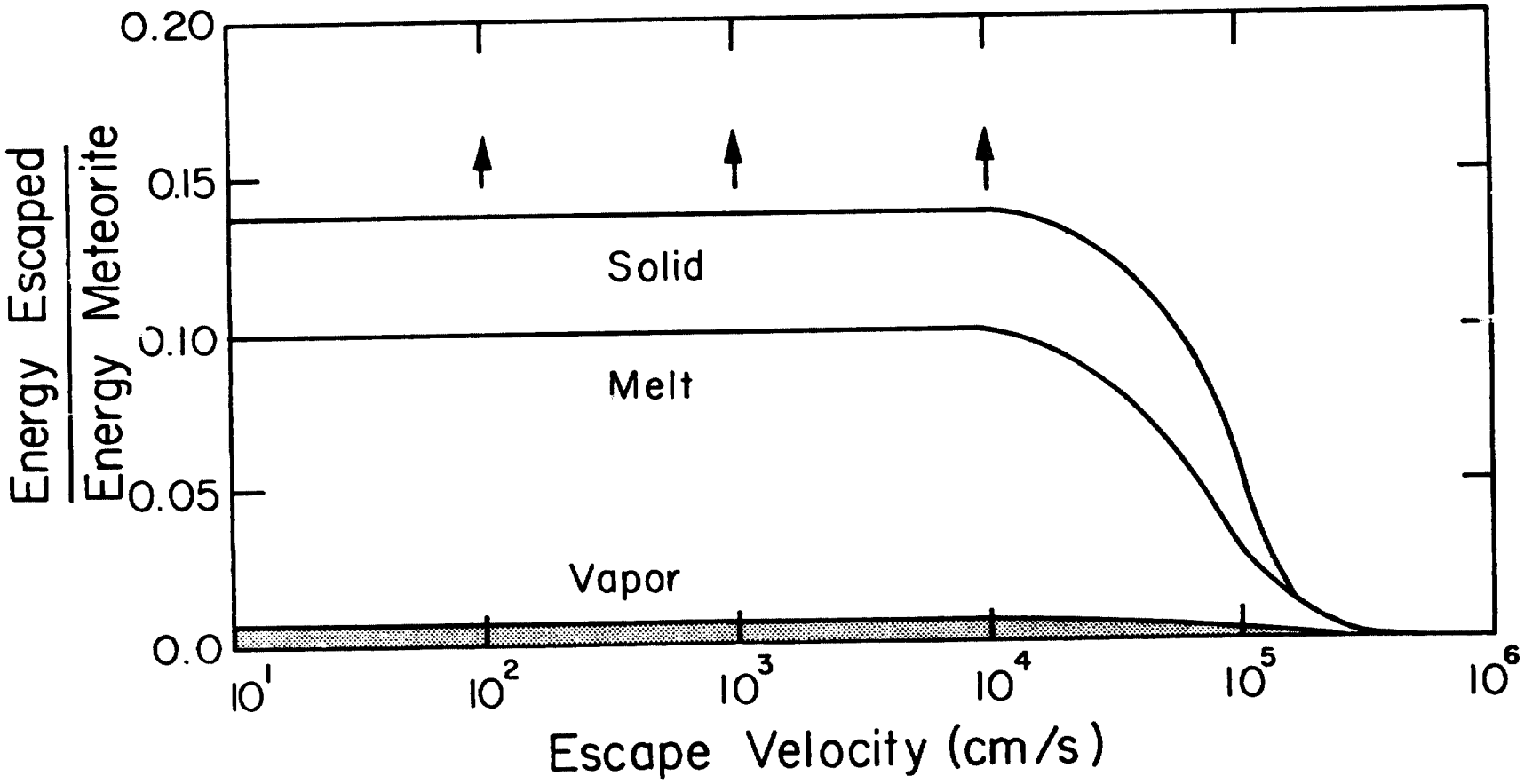
0.20
0.15
0.10
0.05
0.0
Energy Escaped / Energy Meteorite
Solid
Melt
Vapor
10^1
10^2
10^3
10^4
10^5
10^6
Escape Velocity (cm/s)

Fig. 6

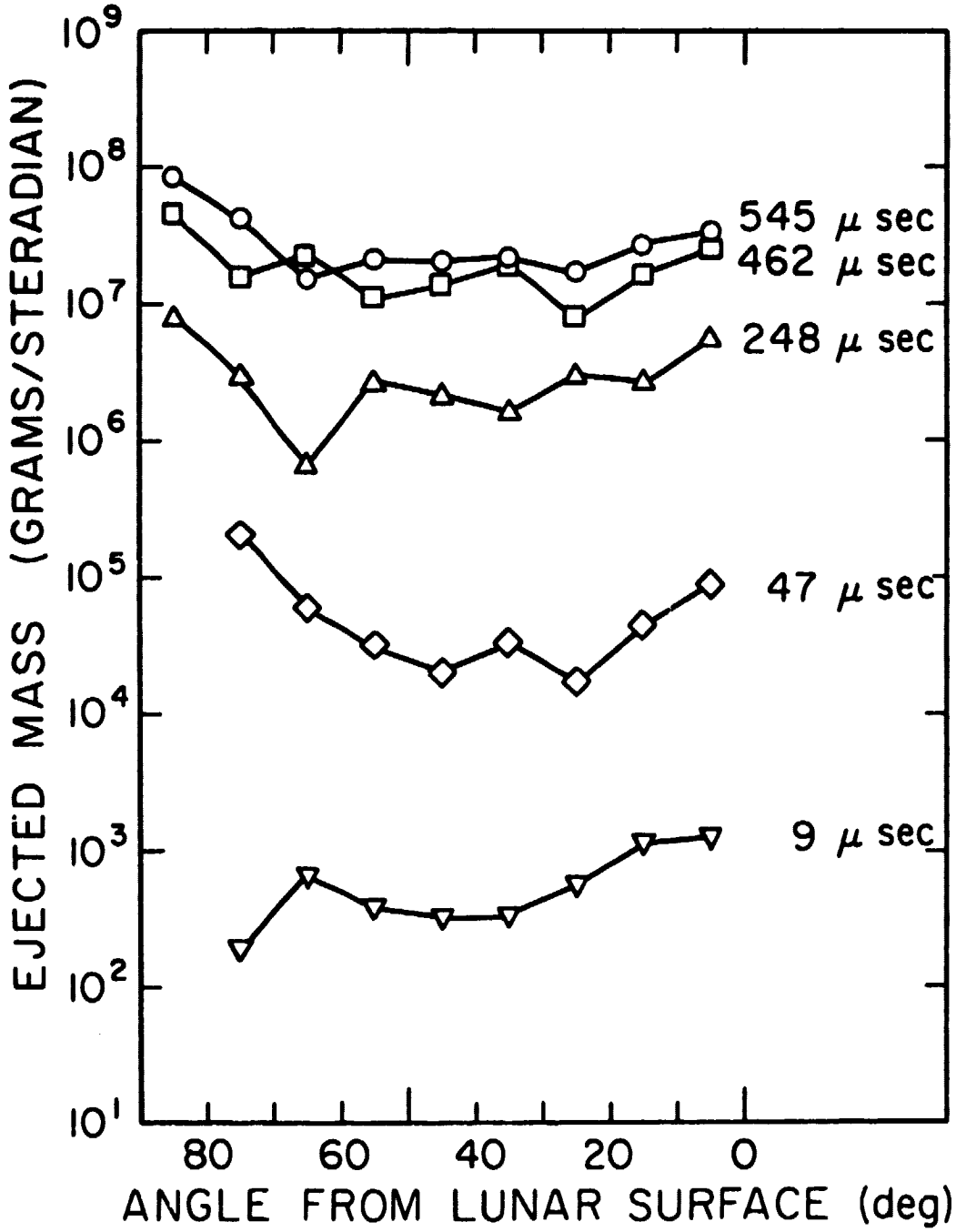
EJECTED MASS (GRAMS/STERADIAN)
10^9
10^8
10^7
10^6
10^5
10^4
10^3
10^2
10^1
545 μ sec
462 μ sec
248 μ sec
47 μ sec
9 μ sec
80
60
40
20
0
ANGLE FROM LUNAR SURFACE (deg)

Fig. 7

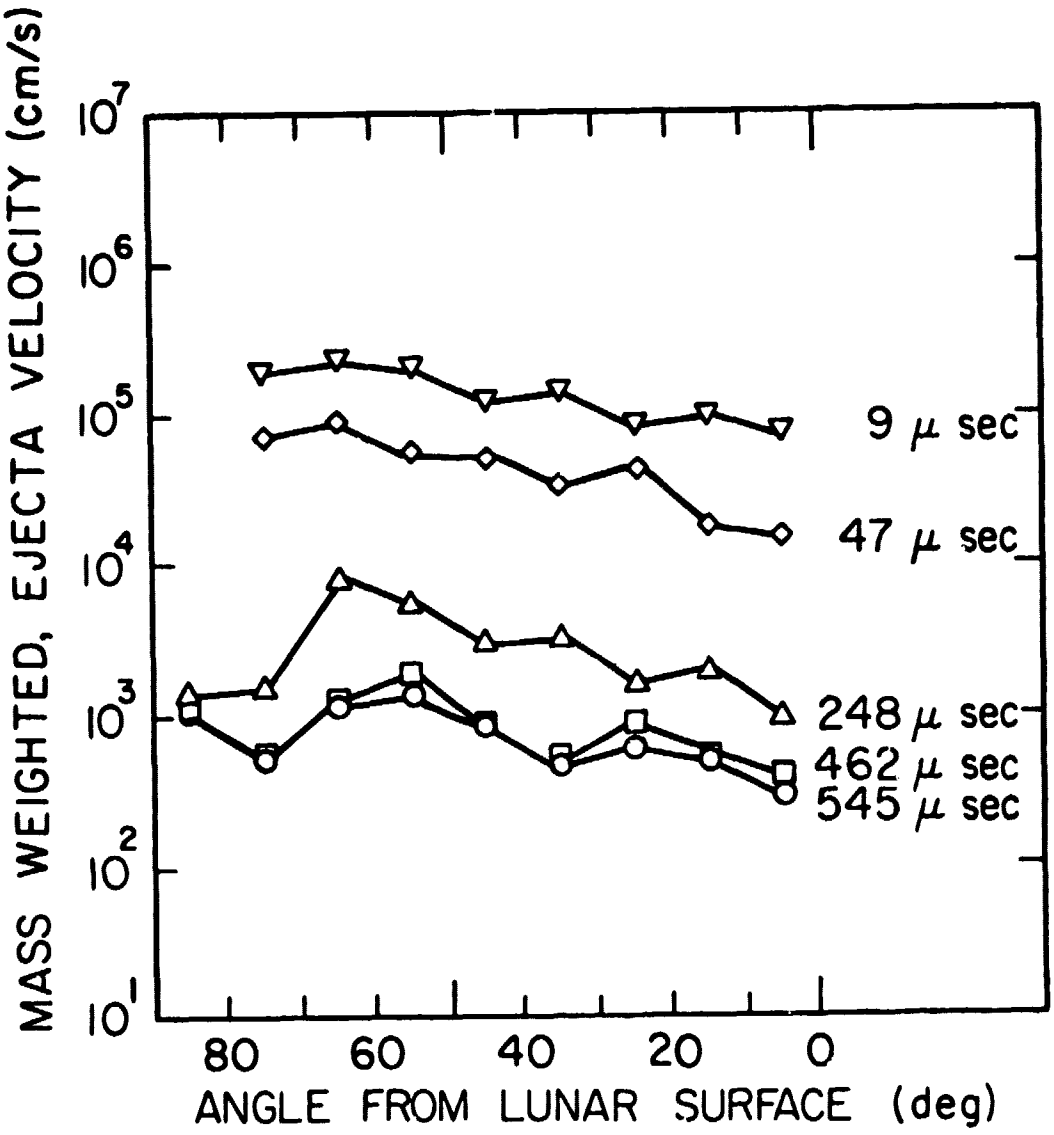
MASS WEIGHTED, EJECTA VELOCITY (cm/s)
10^7
10^6
10^5
10^4
10^3
10^2
10^1
9 μ sec
47 μ sec
248 μ sec
462 μ sec
545 μ sec
80
60
40
20
0
ANGLE FROM LUNAR SURFACE (deg)

Fig. 8

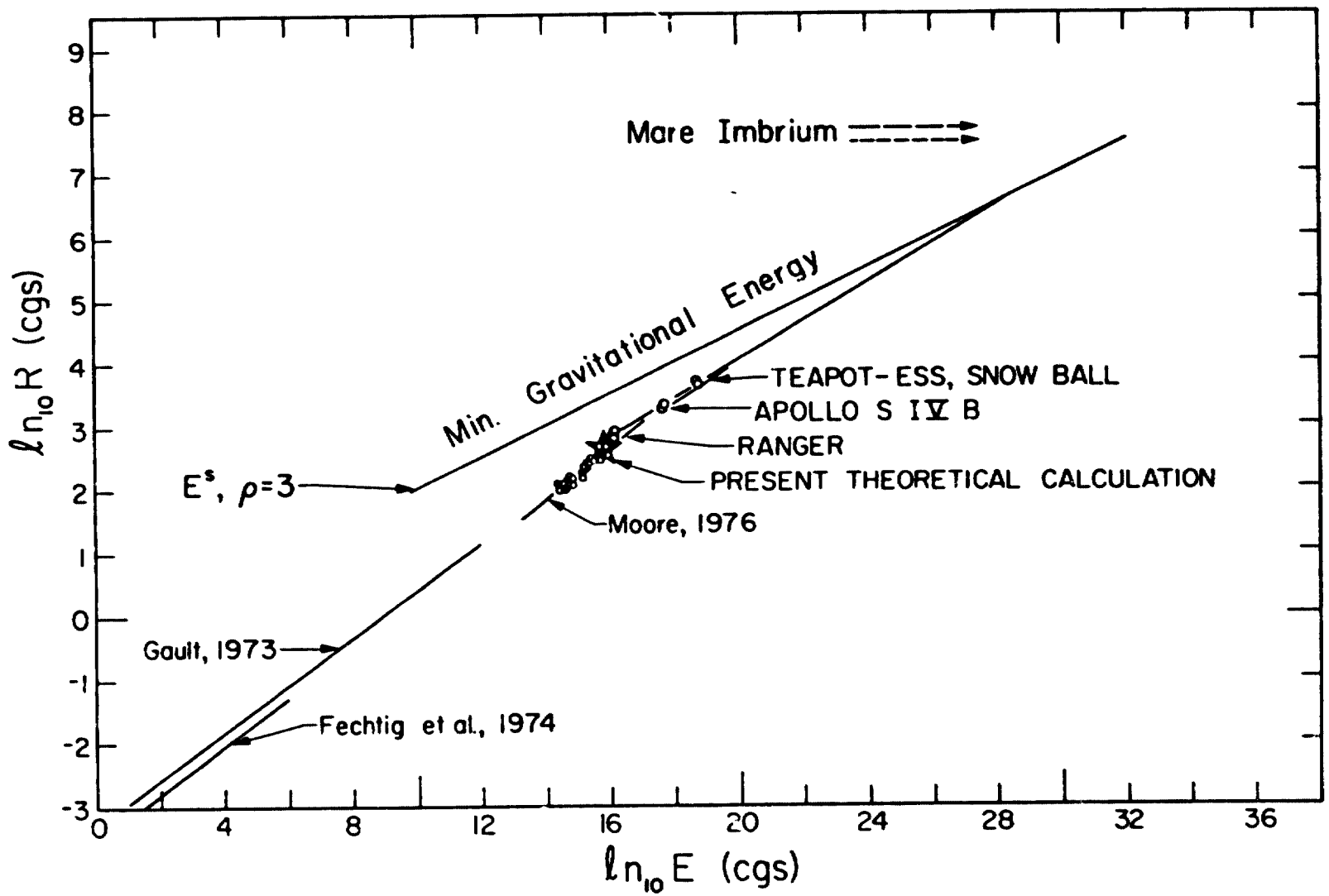
Mare Imbrium
Min. Gravitational Energy
TEAPOT-ESS, SNOW BALL
APOLLO S IV B
RANGER
PRESENT THEORETICAL CALCULATION
Moore, 1976
E^s, ρ=3
Gault, 1973
Fechtig et al., 1974
ℓn10 R (cgs)
ℓn10 E (cgs)
9
8
7
6
5
4
3
2
1
0
-1
-2
-3
0
4
8
12
16
20
24
28
32
36

Fig. 9

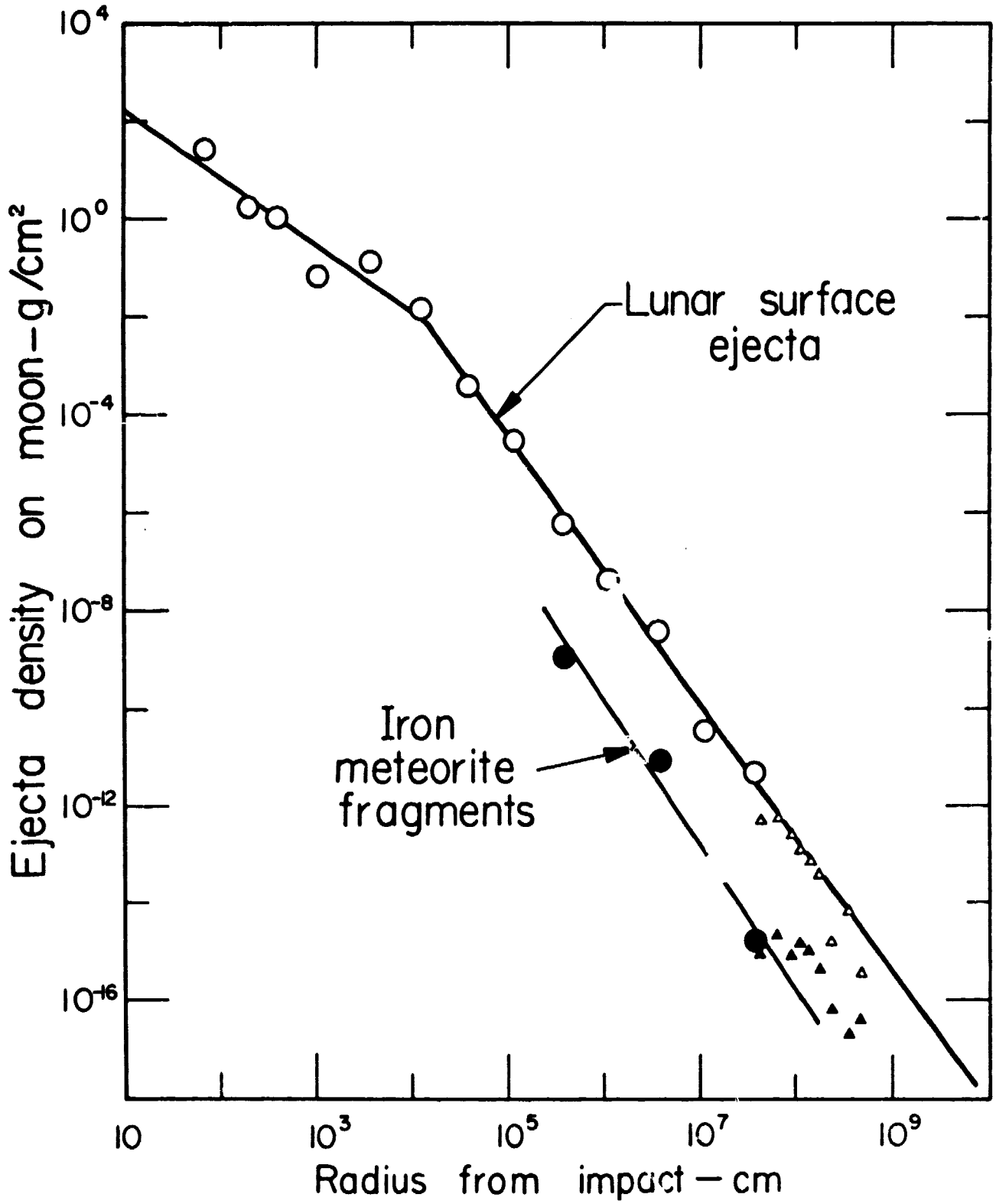
Ejecta density on moon – g/cm²
10⁴
10⁰
10⁻⁴
10⁻⁸
10⁻¹²
10⁻¹⁶
Lunar surface ejecta
Iron meteorite fragments
10
10³
10⁵
10⁷
10⁹
Radius from impact – cm

Fig. 10